RSC Advances

PAPER

View Article Online
View Journal | View Issue

Cite this: *RSC Adv.*, 2022, **12**, 921

Magnetic nanoprobes for rapid detection of copper ion in aqueous environment by surface-enhanced Raman spectroscopy†

Min-Ying Hsieh and Po-Jung Huang *

Excessive copper ions in drinking water could cause serious health issues, such as gastrointestinal disorders and cirrhosis, and they are associated with Alzheimer's disease. ICP-OES, ICP-MS, and AAS are the most common methods of copper ion determination. However, the high cost of sample preparation and labor limit the possibility of on-site detection. In this study, rapid monitoring of copper ion through the SERS technique was evaluated. Fe_3O_4@SiO_2–Ag–4MBA nanoparticles were investigated as SERS-activated magnetic nanoprobes. These magnetic nanoprobes underwent superparamagnetism for rapid aggregation in seconds and provided selectivity in sensing copper ions. According to the dose–response curve of the SERS spectra, the limit of detection (LOD) was 0.421 ppm and the dynamic range was from 0.5 to 20 ppm in the presence of other metal ions. Copper ion detection through SERS was highly correlated with ICP-OES (R^2 = 0.95, slope = 0.974). These results demonstrate that magnetic nanoprobes may ultimately be used in a platform for on-site detection.

Received 9th October 2021
Accepted 14th December 2021

DOI: 10.1039/d1ra07482b

rsc.li/rsc-advances

1. Introduction

Copper is a required trace element in organisms, especially for the regulation of many cellular enzymes. For instance, hematopoiesis in humans relies on ceruloplasmin, a copper ion-containing protein, for the oxidation of Fe^{2+}.[1,2] Although copper ion plays an important role in organisms, uptake of excessive copper ion can induce acute toxicities, resulting in diarrhea, nausea, and vomiting.[3] Moreover, chronic toxicities of copper ion significantly impact the viscera and the central nervous system, especially the brain, leading to Alzheimer's disease[4] and Parkinson's disease.[5] For example, Abbaoui *et al.* reported that Cu^{2+} damages the neuron system and the decreased locomotor performance once the uptake dose of Cu^{2+} is over 10 mg kg^{-1} BW.[6] The Taiwan Environmental Protection Agency (EPA) has set health advisory levels for copper ion in drinking water at 1 ppm.[7] Therefore, the development of a rapid and sensitive method for copper ion detection has attracted considerable attention.

Traditional techniques for Cu^{2+} detection from wastewater are not suitable for on-site detection, such as inductively coupled plasma optical emission spectroscopy (ICP-OES), mass spectroscopy, and atomic absorbance spectroscopy (AA). In practice, ICP-OES and AA are used for Cu^{2+} concentrations within the ppm level. Mass spectroscopy has a lower detection limit, approaching ppb level.[8–10] Researchers are currently investigating alternative detection platforms, including electrochemical, fluorescence, and colorimetric methods. Although electrochemical[11,12] and fluorescence methods[13] provide high sensitivity for Cu^{2+} in water samples, these two approaches require a complex operation process and high-cost equipment.[14,15] In addition, most colorimetric probes for Cu^{2+} are processed under organic solvent because of the organic dyes employed as probes. Recently, silver or gold nanoparticles were reported to display distance-dependent optical properties for rapid detection of Cu^{2+}. For example, Lou *et al.* designed $S_2O_3^{2-}$ decorated Ag/Au nanoprobes to detect Cu^{2+} based on color change.[16] Xiang *et al.* presented NTBL as a colorimetric chemosensor, showing high selectivity for Cu^{2+} in aqueous solution.[17] However, the salt present in aqueous solutions could interrupt the aggregation of nanoprobes, affecting copper ion concentration detection.[18] There is a need to develop a detection platform with rapid detection, high selectivity, and low interference for Cu^{2+} detection.

Raman spectroscopy is a convenient technique for molecular detection through inelastic light scattering in an aqueous sample. However, the intensity of Raman scattering is extremely low because little inelastic light scattering occurs naturally. To improve the Raman signal, metallic nanoparticles, such as silver or gold nanoparticles, create plasmonic 'hotspots' through aggregation.[19] Other heavy metals, such as As^{3+},[20] Hg^{2+},[21,22] Pb^{2+},[22] and Cr^{6+},[23] in aqueous solution are detected using the SERS technique. The use of chelator and organic linkers are common strategies to induce the aggregation of nanoparticles through chelation. Li *et al.* designed stimuli-response Raman reporters for simultaneous detection of Cu^{2+}

Institute of Environmental Engineering, National San Yat-sen University, Kaohsiung 80424, Taiwan. E-mail: pjhuang@mail.nsysu.edu.tw

† Electronic supplementary information (ESI) available. See DOI: 10.1039/d1ra07482b

and HClO through covalent bonding.[24] Inspired by the above report, we developed functional magnetic nanoparticles, Fe_3O_4@SiO_2–Ag–4MBA, which were designed as probes for copper ion detection by surface-enhanced Raman spectroscopy (SERS). This approach monitors the signal increases through the formation of 'hotspots' with simultaneous magnetic field application and copper ion chelation. Magnetic nanoprobes exhibit superparamagnetism to achieve rapid aggregation, and 4-MBA composes the carboxylic acid group, which can react with copper ion through chelation. On the other hand, 4-MBA contributes to the selective molecular aggregation with copper ions, leading to the enhanced Raman signal of 4-MBA. As a result, the quantitative results are investigated by a significant change in Raman spectra accomplished by increasing the signal intensity of 4-MBA after Cu^{2+} induction. This demonstrates that the described SERS magnetic nanoprobes are able to capture and sense Cu^{2+} for this magnetic assay development.

2. Experimental

2.1 Reagents and materials

Silver nitrate reagent plus ($AgNO_3$, 99.85%), sodium borohydride ($NaBH_4$, 99%), and copper(II) nitrate trihydrate (99%) were purchased from Acros Organics. Thiosalicylic acid ($C_7H_6O_2S$, 98%) and iron(II) chloride tetrahydrate ($FeCl_2 \cdot 4H_2O$, 98%) were purchased from Alfa Aesar. Silver nitrate solution 0.01 N and hydrochloric (HCl) were purchased from Honeywell Fluka. Tin(II) chloride dihydrate ($SnCl_2 \cdot 2H_2O$, 98%) was purchased from Scharlau. Copper sulfate ($CuSO_4 \cdot 5H_2O$, 98%) was purchased from Choneye pure chemicals. Cupric chloride dihydrate ($CuCl_2 \cdot 2H_2O$, 99%) was purchased from HSE pure chemicals. 4-Mercaptobenzoic acid (4-MBA, >95%) was purchased from TCI. Tetraethyl orthosilicate (TEOS, 98%) was purchased from Aldrich. Ammonium hydroxide (NH_4OH, 28–30%) was purchased from MTEDIA. Iron(III) chloride hexahydrate ($FeCl_3 \cdot 6H_2O$, >98%) was purchased from Sigma Aldrich. All solutions were prepared using high-purity water with a resistance of 18 MΩ cm. All chemicals used were analytical grade or of the highest purity available.

2.2 Synthesis of 4MBA–Ag nanoparticle probe (4MBA–AgNPs)

First, 200 mL of 10^{-4} M $AgNO_3$ solution was prepared and then 0.02 g $NaBH_4$ was added into the solution. Next, the solution was stirred vigorously for 5 minutes, and the solution color turned light-yellow. Then, 600 μL of 10^{-3} M 4-MBA solution was added into the AgNP solution. The solution was adjusted to pH 7.4 and stirred continuously for 1 h 4-MBA will self-assemble onto the AgNP surface. All the above procedures were prepared in an ice bath.

2.3 Synthesis of Fe_3O_4@SiO_2–Ag nanoparticle probe (Fe_3O_4@SiO_2–AgNPs)

$FeCl_2 \cdot H_2O$ (1.8 g) and $FeCl_3 \cdot 6H_2O$ (4.8 g) were mixed in 100 mL DI water. Next, the mixture was stirred vigorously under a N_2 atmosphere until the salt dissolved completely. Then, 28% NH_4OH was added slowly into the reaction mixture at room temperature and stirred for 1 h. After the reaction was completed, the black precipitate, Fe_3O_4, was separated using a magnetic field. The isolated Fe_3O_4 nanoparticles were washed with DI water several times and redispersed in a 100 mL ethanol solution containing 10 mL of 28% NH_4OH and 6 mL TEOS. The polymerization of SiO_2 was spontaneously processed onto the surface of magnetic nanoparticles under 2 hours of sonication. The residue was cleaned with anhydrous ethanol three times. The third step was to deposit Ag onto the Fe_3O_4@SiO_2 NPs through reduction. $SnCl_2$ and HCl were added to the solution containing Fe_3O_4@SiO_2 NPs for activation. Then, silver ammonia solution was mixed with Fe_3O_4@SiO_2 NP solution, forming Fe_3O_4@SiO_2–AgNPs. The final step was to introduce SERS-activated molecules, 4-MBA, onto the Fe_3O_4@SiO_2–AgNPs as a magnetic probe. Fe_3O_4@SiO_2–AgNPs were resuspended in anhydrous ethanol and mixed with 50 mL of 10^{-3} M 4-MBA solution under 2 hours self-assembly reaction. The reacted NPs were collected as Fe_3O_4@SiO_2–AgNPs probe for further sensing purposes.

2.4 Characterization of Fe_3O_4@SiO_2–AgNP probe

The chemical structure of Fe_3O_4@SiO_2–AgNPs was characterized by Fourier transform infrared spectroscopy (FT-IR, Nicolet iS5), X-ray diffraction (XRD, Bruker D8), and X-ray photoelectron spectroscopy (XPS, VG Scientific ESCALAB 250). The morphology of NPs was observed by transmission electron microscopy (TEM, JEOL-2100F). The magnetic properties were measured using a superconducting quantum interference device (SQUID, MPMS-XL7, QUANTUM DESIGN, America). Particle size and distribution were determined by Nano-ZS.

2.5 Copper ion detection

This study aimed at developing 4-MBA-activated nanoprobes for copper ion detection. 4-MBA not only contributes to the selectivity toward copper ion but also plays the role of Raman reporter. The wavelength of the laser was 532 nm for launching surface plasma around the surface of silver nanoparticles. Then, the generated surface plasma is delivered to 4-MBA. The characteristic peaks of 4-MBA are present in the Raman spectrum because of loss of Laser energy. In addition, the intensity of 4-MBA peaks corresponds to the level of aggregation of nanoprobes, which is caused by various concentrations of copper ions. The transmission grating beam splitter had 1800 grooves per mm. The scan range was from 1000 to 2000 cm^{-1}. All experimental results were recorded under 100 seconds of exposure time within one scan, and these recorded results were analyzed by Labspec5 software. To validate the concentration of copper ions determined using SERS, the prepared copper ion sample was confirmed by inductively coupled plasma optical emission spectrum (ICP-OES, Perkin-Optima 7000 DV).

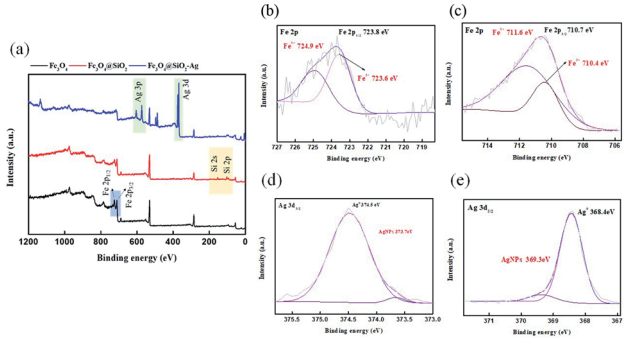

Fig. 1 XPS spectra of the Fe_3O_4@SiO_2–Ag composite nanoparticles. (a) Survey spectrum; (b) Fe $2p_{1/2}$; (c) Fe $2p_{3/2}$; (d) Ag $3d_{3/2}$; (e) Ag $3d_{5/2}$.

3. Results and discussion

3.1 Characterization of Fe_3O_4@SiO_2–AgNP probe

Fig. 1 shows the XPS results for the Fe_3O_4@SiO_2–AgNP composite. The survey spectrum of Fe_3O_4 (Fig. 1a) showed two photoelectron peaks at 710.7 and 723.8 eV corresponding to Fe $2p_{3/2}$ and Fe $2p_{1/2}$, respectively.[25,26] The newly added peaks in Fe_3O_4@SiO_2 at 103.5 eV were assigned as SiO_2. In addition, the binding energies at 368 and 374 eV observed in the survey spectrum of Fe_3O_4@SiO_2–AgNPs were demonstrated as Ag $3d_{5/2}$ and Ag $3d_{3/2}$. Fig. 1b and c present the Fe 2p spectrum of Fe_3O_4@SiO_2–AgNPs. The peaks at 710.4 and 723.6 eV were contributed by Fe^{2+}, and the peaks at 711.6 and 724.9 eV were assigned as Fe^{3+}.[27] The ratio of the respective areas under Fe^{2+} and Fe^{3+} peaks was 1 to 1.6, which is ascribed to Fe_3O_4. Fig. 1d shows the high-resolution Ag 3d spectrum. Binding energy at 368.4 and 374.5 eV is ascribed to metallic silver (Ag^0) on Fe_3O_4@SiO_2–AgNPs.[28] In addition, shoulder peaks located at 369.3 and 373.4 eV were related to AgNPs.[29]

Fig. 2a presents the XRD patterns of Fe_3O_4, Fe_3O_4@SiO_2, and Fe_3O_4@SiO_2–AgNPs. The main peaks of Fe_3O_4 within the inverse spinel phase presented at 30.4°, 35.7°, 43.4°, 53.8°, 57.3°and 62.9°, which correspond to (2 0 0), (3 1 1), (4 0 0), (4 2 2), (5 1 1) and (4 4 0).[30,31] In the case of Fe_3O_4@SiO_2, a newly broadened peak was observed between 20 and 30°, which was contributed by amorphous SiO_2.[32,33] The diffraction pattern of Ag can be characterized in the XRD spectrum of Fe_3O_4@SiO_2–AgNPs. The additional angles of 38.3°, 44.5°, 64.6°, and 77.5° correspond to AgNPs within FCC structure, marked as (1 1 1), (2 0 0), (2 2 0) and (3 1 1).[34,35] The results, in line with previous research, reflected that AgNPs were successfully modified onto the Fe_3O_4@SiO_2 surface. Fig. 2b demonstrates the magnetic properties of Fe_3O_4@SiO_2–AgNPs in each modification. Even though magnetization saturation (Ms) of Fe_3O_4 decreased after multiple modifications, there is no observation of magnetic hysteresis loop (the coercivity and remanence are zero). This indicated that the synthesized Fe_3O_4, after multiple steps of modifications, still exhibited superparamagnetism, and aggregations of magnetic nanoprobes easily formed in a few seconds (inset photo in Fig. 2b).

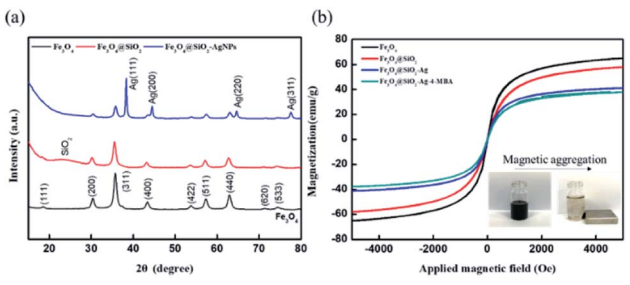

Fig. 2 Characterization of Fe_3O_4@SiO_2–Ag composite nanoparticles. (a) XRD spectrum; (b) SQUID analysis (inset shows magnetic aggregation of probes).

Fig. 3a and b present DLS results for particle size and distribution of AgNPs and Fe_3O_4 NPs. 4-MBA–AgNPs showed slightly larger average particle size (14.63 ± 2.14 nm, PDI = 0.210) than the bare Ag spherical NPs, as shown in Fig. 3c (12.95 ± 1.58, PDI = 0.179), because of self-assembled 4-MBA molecules. Meanwhile, the average size of Fe_3O_4 particles also increased from 24.79 ± 1.58 nm (PDI = 0.138) to 31.84 ± 2.78 nm (PDI = 0.254) due to the formation of the 7 nm-thick SiO_2 layer. Based on the TEM image, the appearance of bare Fe_3O_4 NPs (Fig. 3d) was spherical, and their particle size ranged from 13 to 15 nm. Superparamagnetic property is attributed to the critical size range of magnetic nanoparticles between 10 to 15 nm,[36] proving the superparamagnetism of Fe_3O_4@SiO_2–AgNPs. Fe_3O_4@SiO_2–AgNPs were synthesized by the Stöber method, resulting in the formation of core–shell structures, as shown in Fig. 3e. The dark region in the core–shell is Fe_3O_4, and the gray region is SiO_2; small particles on the SiO_2 surface are silver nanoparticles.[37–39] The EDS results also indicated that the central area has Si and Fe elements, and the outer layer of the core–shell structure reflects Ag and Si elements. Based on these analytic results from XRD, XPS, DLS, and TEM, SERS-activated Fe_3O_4@SiO_2–AgNP probes were successfully synthesized.

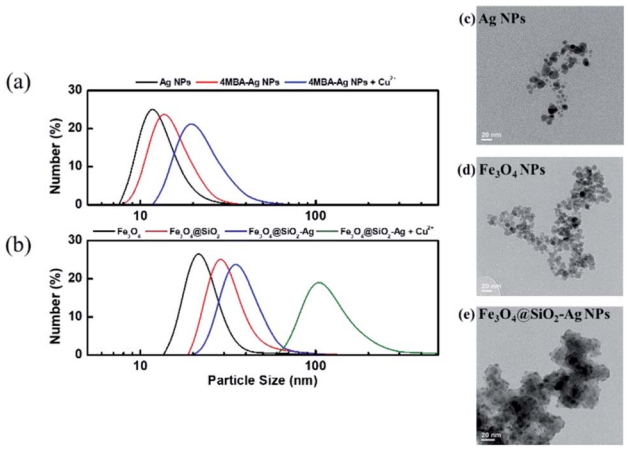

Fig. 3 Particle size and morphology of AgNPs and Fe_3O_4@SiO_2–Ag composite nanoparticles before/after copper ion-induced aggregation. Size distribution of (a) AgNPs, 4 MBA–AgNPs, and 4 MBA–AgNPs + Cu^{2+}; (b) Fe_3O_4 NPs, Fe_3O_4@SiO_2 NPs, Fe_3O_4@SiO_2–Ag, and Fe_3O_4@SiO_2–Ag + Cu^{2+}; TEM images of (c) AgNPs; (d) Fe_3O_4 NPs; and (e) Fe_3O_4@SiO_2–AgNPs (scale bar: 20 nm).

3.2 Copper ion detection using SERS

4-MBA was the Raman reporter, which emitted surface-enhanced Raman signal (SERS) after Fe_3O_4@SiO_2–AgNP probes aggregated, called a hot spot. The generation of hot spots can be determined by magnetic field application and copper ion introduction. Fig. 4a presents the Raman spectrum of 4-MBA with or without copper ion introduction. There were two specific peaks, 1080 cm^{-1} and 1584 cm^{-1}, corresponding to C–H in-plane bending and C–C stretching vibrational modes of 4-MBA, respectively.[40,41] Once the magnetic field was applied for aggregation, the SERS peak intensities of the vibrational mode at 1080 and 1584 cm^{-1} increased compared to a plain solution without magnetic field. Further, the introduction of 30 ppm copper ion would additionally enhance the intensity of SERS peaks. This indicated that a magnetic field would physically generate a hot spot, resulting in improved Raman peak intensities. Then, copper ion was chelated with a carboxylic acid of 4-MBA for additional aggregation between magnetic nanoprobes. Fig. 3a and b prove that the average particle size of 4-MBA–AgNPs and Fe_3O_4@SiO_2–Ag–MBA NPs became larger after adding copper ion, from 14.63 ± 2.14 nm (PDI = 0.210) to 21.57 ± 1.97 nm (PDI = 0.48) and from 37.08 ± 1.33 nm (PDI = 0.191) to 124.37 ± 8.75 nm (PDI = 0364), respectively. Therefore, Fe_3O_4@SiO_2–Ag–MBA NPs can be used as a probe for sensing copper ions in an aqueous environment.

To optimize the sensitivity of copper ion detection, we relied on the SERS peak at 1584 cm^{-1} because of its high intensity after copper-induced aggregation. According to the strategy of copper ion detection, the concentration of the modifier (4-MBA) and the magnetic probe/copper ion ratio play essential roles. Fig. 4b illustrates the concentration of 4-MBA for copper ion detection. The concentration of 4-MBA was set as 5×10^{-4} M, 5×10^{-3} M, 10^{-3} M, and 10^{-2} M, respectively. A low amount of 4-MBA was unable to generate sufficient chelation between magnetic nanoprobes, resulting in less aggregation and low SERS signal intensity, while a higher concentration of 4-MBA caused molecular overlapping. Consequently, the copper ion was hard to chelate with 4-MBA and even reduced the SERS peak signal.[42] The optimized concentration of the modifier was 10^{-3} M for further preparation. Fig. 4c presents the Raman signal intensity under different volume ratios between magnetic nanoprobes and copper ion. The best performance was the ratio of 1 : 0.4 (magnetic nanoprobes/copper ion).

The stock magnetic nanoprobe prepared from the optimized condition was mixed with different concentrations of copper ions from 0 to 30 ppm. The SERS peak intensities of the vibrational mode at 1080 and 1584 cm^{-1} as a function of concentration are shown in Fig. 5a. The trend of copper ion concentration and SERS signal intensity at 1584 cm^{-1} followed a dose–response curve, where the MBA intensity can be distinguished over 1 ppm and saturated around 30 ppm. A better linear correlation result was observed for concentrations ranging from 0.5 to 20 ppm ($R^2 = 0.99$), meaning 30 ppm would be close to the copper ion detection upper limit.

To confirm the SERS signal was launched by copper-induced aggregation, 2TSA, the isomer of 4-MBA, was selected as an alternative modifier decorating Fe_3O_4@SiO_2–AgNPs. Fig. 6 demonstrated the Raman spectrum under different SERS modifiers. The SERS peaks for Fe_3O_4@SiO_2–Ag–4-MBA NPs were more obvious than for Fe_3O_4@SiO_2–Ag–2TSA NPs. The carboxyl acid group in 4-MBA is positioned toward the outer region, resulting in an effective triggering of copper-induced aggregation. Meanwhile, the carboxyl acid group of 2TSA is at the *ortho* position, which indicated this activated site is positioned toward the inside. The steric hindrance of the chemical structure usually reduces the reaction speed, and the degree of influence of the *ortho* position would be greater than the *para* position.[43] This explanation was further proved through the colorimetric method using 4MBA@Ag and 2TSA@Ag, as shown in Fig. S1.† 4MBA@Ag successfully induced aggregation because of the color change from bright yellow to red, while 2TSA@Ag did not effectively trigger aggregation. In the UV spectrum, 4MBA@Ag showed a distinct red-shift with increasing concentration of copper ion, compared with 2TSA@Ag probes. Consequently, Fe_3O_4@SiO_2–Ag–2TSA NPs have no response for copper ion detection through the Raman signal. It was demonstrated that the steric effect of modifiers could significantly affect copper ion detection.

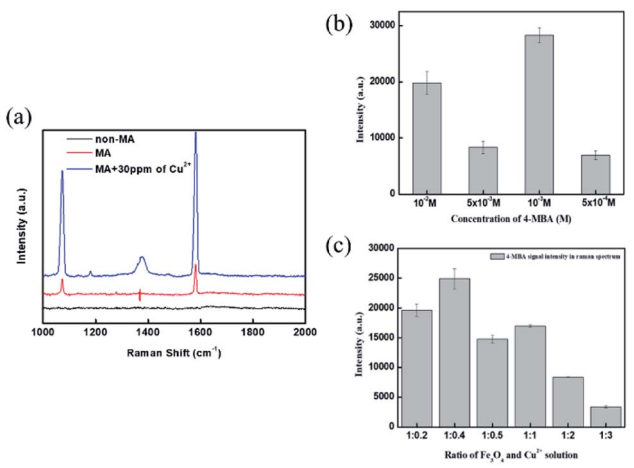

Fig. 4 Copper ion detection using Fe_3O_4@SiO_2–AgNP probe. (a) Raman spectrum of 4 MBA before/after copper ion induction using 10^{-3} M 4-MBA as a modifier (MA is magnetic aggregation); (b) concentration effect of 4-MBA; (c) ratio of Fe_3O_4@SiO_2–AgNPs and copper ion solution (total volume: 5 mL).

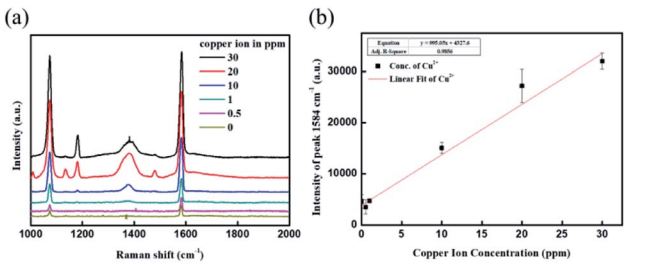

Fig. 5 Detection of different concentrations of copper ions using Fe_3O_4@SiO_2–AgNPs probe. (a) Raman spectrum of 4-MBA under different concentrations of copper ions; (b) linear calibration curve of copper ion based on the intensity of the peak at 1584 cm^{-1}.

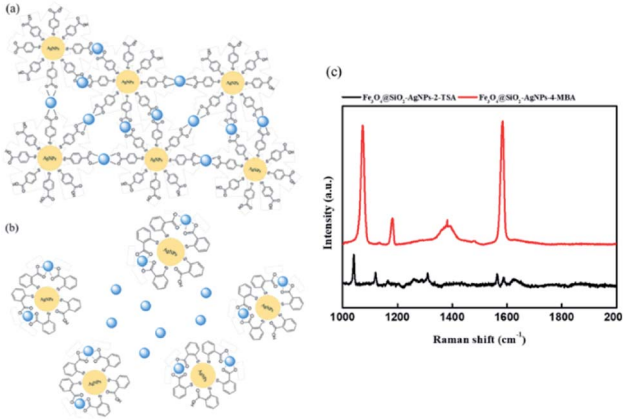

Fig. 6 The steric effect of modifier (4-MBA and 2-TSA) on Fe_3O_4@SiO_2–AgNP probe for copper ion response. Scheme of (a) 4-MBA-induced aggregation and (b) 2-TSA-induced aggregation; (c) Raman spectrum of Fe_3O_4@SiO_2–AgNPs–4MBA and Fe_3O_4@SiO_2–AgNPs–2TSA after copper ion-induced aggregation (copper ion concentration: 30 ppm).

3.3 Interference of copper ion detection through Fe_3O_4@SiO_2–Ag–4MBA NPs

The strategy of Fe_3O_4@SiO_2–Ag–4MBA NPs for copper ion detection follows chelation of the carboxyl acid group on 4MBA. Therefore, other transition metals that exist in wastewater would potentially interfere with the detection. Fig. 7 presents the intensity of the SERS peak at 1584 cm^{-1} after introducing different types of metal ions. Copper ion exhibited a more sensitive response to Fe_3O_4@SiO_2–Ag–4MBA NPs, and second was lead ion. Other metal ions introduced, like Fe^{2+}, Ni^{2+}, and Zn^{2+}, performed similar SERS response as the control groups, which are DI water without any metal ion. The results indicated that Fe_3O_4@SiO_2–Ag–4MBA NPs can selectively detect copper and lead ions. Further, the response of Fe_3O_4@SiO_2–Ag–4MBA NPs toward copper ion and lead ion was investigated, and the concentration ranges of these two metal ions were from 0 to 30 ppm, as shown in Fig. 7b. The detection range for lead ion was narrower than for copper ion because lead ion-induced Raman signal achieved saturation soon after 1 ppm. This obvious difference was caused by chelating types. The chelation between the metal ion and the chelating agent could achieve equilibrium. Therefore, the stability of the chelating complexes determined the level of aggregation of magnetic nanoprobes and the stimulation of SERS signals. Copper ions and carboxylic acid prefer to form bidentate chelates,[44] which illustrates that copper ion requires two carboxyl acid groups to stabilize the chelating complex. Copper ions could process spontaneous aggregation of magnetic nanoprobes due to maintenance of the stability for copper-based chelation complexes. In contrast, lead ion belongs to monodentate chelation,[44] and lead ion only induced partial aggregation of magnetic nanoprobes. Therefore, the SERS peak intensity was reflected in a slightly increasing manner by added lead ions compared to the bare magnetic aggregation. Consequently, Fe_3O_4@SiO_2–Ag–4MBA NPs have selectivity for copper ion, with the highest sensitivity.

Apart from metallic ions, the SERS signal was also influenced by anions. Fig. S2† presents copper ion detection under different anions using 4MBA@Ag. The results show different dose–response curves, indicating different sensitivities and linear detection ranges for copper ion with different salts. Copper ion detection in the presence of chloride had higher sensitivity than with sulfate. In addition, the linear range of copper ion detection in the presence of sulfate was wider than with chloride. The possible reason is the Hofmeister series, which influences the hydration ability of copper ion compounds.[18] In addition, sulfate (SO_4^{2-}) exhibit strong hydration ability and greater hydrogen bonding toward water molecules, resulting in reduced solubility of copper sulfate.[45,46] It was demonstrated that free copper ion determines the sensitivity and linear detection range using 4MBA@Ag nanoprobes. Fig. 7c shows the anion effect for copper ion using Fe_3O_4@SiO_2–Ag–4MBA NPs. The Raman results demonstrated that the trend of sensitivity and linear detection range were similar

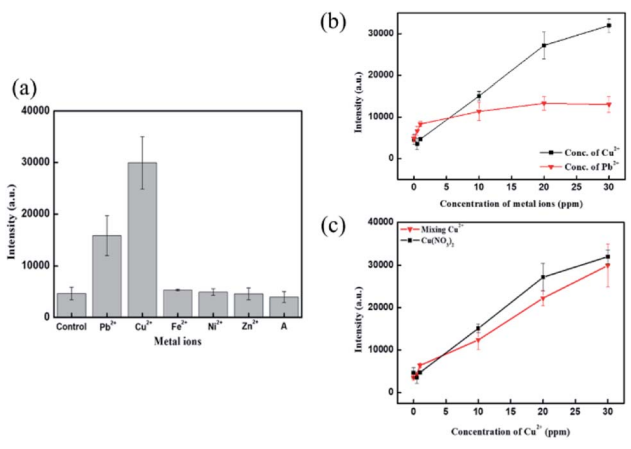

Fig. 7 Environmental effect of copper ion detection using Fe_3O_4@SiO_2–AgNPs probe. (a) SERS response in different metal ions (copper ion concentration: 30 ppm); (b) SERS response of copper and lead ion in different concentrations; (c) anion effect in different concentrations of copper ions.

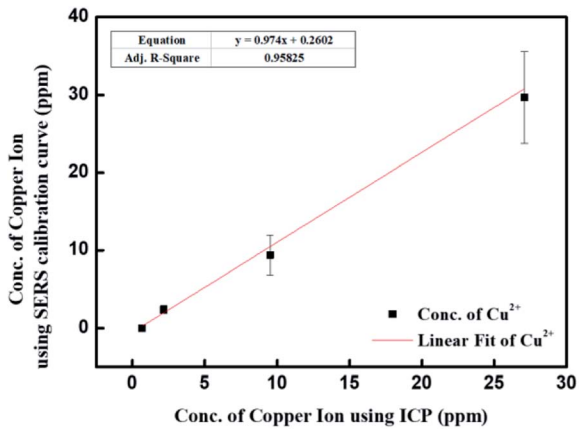

Fig. 8 Comparison of copper ion detection through ICP and SERS analysis.

Table 1 Comparison of colorimetric sensors for the detection of Cu^{2+}

Methods	Analytical range (μM)	Limit of detection (μM)	Reaction time	Ref.
Colorimetric	0.1–100	25×10^{-3}	30 min	47
Colorimetric	1–1000	1	30 min	48
Fluorescent	0.25–10	29.5×10^{-3}	3 s	13
Fluorescent	0.01–1.1	6×10^{-3}	1 min	49
Electrochemical	1–10	N/A	5 min	11
Electrochemical	0.001–100	0.3×10^{-3}	1 h	12
SERS	3.7–148.7	3.13	10 s	This study

either in copper nitrate or the mixed copper salts. It was illustrated that the application of magnetic field would effectively aggregate Fe_3O_4@SiO_2–Ag–4MBA NPs, and then magnetic nanoprobe clusters would be additionally become dense through copper ion introduction. Consequently, the Hofmeister series would be minimized using Fe_3O_4@SiO_2–Ag–4MBA NPs in copper ion detection.

To validate the copper ion concentration using SERS detection, ICP-OES is a reliable tool for the quantification of metal ion. The prepared copper ion concentrations were 0.5, 2, 10, and 30 ppm, respectively. Fig. 8 shows the plot of copper ion concentration through ICP analysis and SERS detection. The slope of linear fitting was close to 1, indicating the precision of copper ion detection through SERS detection in this study. When comparing the results of this study with the other favourable methods shown in Table 1, it can be suggested that the Fe_3O_4@SiO_2–Ag–4MBA-based detection assay approaches the rapid detection of copper ion under a similar analytical range.

4. Conclusion

This study aimed to develop a platform for rapid detection of copper ions in wastewater through Raman spectra without any further pretreatment. Sensitive detection through SERS required generating the detection area, called hot spot, in a wastewater sample. Fe_3O_4@SiO_2–Ag–4MBA NPs can activate the hot spot through magnetic aggregation and copper ion-induced aggregation. Magnetic aggregation was processed by superparamagnetic material-Fe_3O_4, and copper ion-induced aggregation was launched by carboxylic acid chelation. 4-MBA not only provides carboxylic acid chelation with copper ion but also emits the Raman signal after aggregation. The Raman signal increased as a function of copper ion increase. The linearity of detection range was from 0.5 to 20 ppm within a high coordination, and the limit of detection was 0.421 ppm. In addition, it is noted that the error bar at higher concentrations of copper ion is larger than at the lower concentration due to the non-homogeneous nature of the aggregation. On the other hand, the uniform distribution of AgNPs does influence reproducibility. The limit of detection and reproducibility can be improved by other chelators modified on silver nanoparticles. 4-MBA only contributes carboxylic acid for chelating copper ions. Modifiers containing more amines and carboxylic acid in their molecular structure, like polyethyleneimine (PEI) and peptide-containing cysteine, would effectively contribute stronger interaction toward copper ions, leading to higher sensitivity. Magnetic aggregation belongs to active aggregation, which can effectively minimize the anion effect (Hofmeister series) in wastewater. In addition, the carboxylic acid on magnetic nanoprobes determined the selectivity for metal ions through chelation affinity. Copper and lead ion gave significant SERS responses compared with other transition metal ions. Based on bidentate chelation, Fe_3O_4@SiO_2–Ag–4MBA NPs were more sensitive for copper ion in a wide range. Copper ion detection using the SERS method was as precise as ICP-OES. All of the measurements can be done in a couple of seconds, achieving rapid detection. In the near future, these magnetic probes can be integrated with a microfluidic device and a portable Raman spectrometer as a portable device for on-site detection of wastewater.

Author contributions

Po-Jung Huang conceived, planned and supervised the project. Min-Ying Hsieh performed the experiments and interpreted the data. Po-Jung Huang and Min-Ying Hsieh wrote the manuscript.

Conflicts of interest

There are no conflicts to declare.

Acknowledgements

This work was supported by the Ministry of Science and Technology under Project MOST 107-2218-E-110-018-MY3 and MOST 110-2221-E-110-024.

References

1 Z. W. Myint, *et al.*, Copper deficiency anemia: review article, *Ann. Hematol.*, 2018, **97**(9), 1527–1534.
2 T. Kirsipuu, *et al.*, Copper(II)-binding equilibria in human blood, *Sci. Rep.*, 2020, **10**(1), 5686.
3 National Research Council Committee on Copper in Drinking, W., in *Copper in Drinking Water*, National Academies Press (US) Copyright 2000 by the National

Academy of Sciences, all rights reserved, Washington (DC), 2000.
4 H. W. Ejaz, W. Wang and M. Lang, Copper Toxicity Links to Pathogenesis of Alzheimer's Disease and Therapeutics Approaches, *Int. J. Mol. Sci.*, 2020, **21**(20), 7660.
5 M. Bisaglia and L. Bubacco, Copper Ions and Parkinson's Disease: Why Is Homeostasis So Relevant?, *Biomolecules*, 2020, **10**(2), 195.
6 A. Abbaoui, *et al.*, Neuroprotective effect of curcumin-I in copper-induced dopaminergic neurotoxicity in rats: A possible link with Parkinson's disease, *Neurosci. Lett.*, 2017, **660**, 103–108.
7 Environmental Protection Administration, E.Y., *Drinking Water Quality Standards*, 2017.
8 V. Chrastný and M. Komárek, Copper determination using ICP-MS with hexapole collision cell, *Chem. Pap.*, 2009, **63**(5), 512–519.
9 E. J. Santos, *et al.*, Determination of trace metals in electrolytic copper by ICPOES and ICP-MS, *Braz. Arch. Biol. Technol.*, 2005, **48**, 681–687.
10 G. Bagherian, *et al.*, Determination of copper(II) by flame atomic absorption spectrometry after its preconcentration by a highly selective and environmentally friendly dispersive liquid–liquid microextraction technique, *J. Anal. Sci. Technol.*, 2019, **10**(1), 3.
11 M. Lin, *et al.*, Electrochemical detection of copper ion using a modified copolythiophene electrode, *Electrochim. Acta*, 2009, **54**(27), 7012–7017.
12 T. Wu, T. Xu and Z. Ma, Sensitive electrochemical detection of copper ions based on the copper(ii) ion assisted etching of Au@Ag nanoparticles, *Analyst*, 2015, **140**(23), 8041–8047.
13 Y. Wang, *et al.*, Yellow-visual fluorescent carbon quantum dots from petroleum coke for the efficient detection of Cu2+ ions, *New Res. Carbon Mater.*, 2015, **30**(6), 550–559.
14 S. C. Wilschefski and M. R. Baxter, Inductively Coupled Plasma Mass Spectrometry: Introduction to Analytical Aspects. The Clinical biochemist, *Reviews*, 2019, **40**(3), 115–133.
15 K. L. Nuttall, W. H. Gordon and K. O. Ash, Inductively coupled plasma mass spectrometry for trace element analysis in the clinical laboratory, *Ann. Clin. Lab. Sci.*, 1995, **25**(3), 264–271.
16 T. Lou, *et al.*, Colorimetric Detection of Trace Copper Ions Based on Catalytic Leaching of Silver-Coated Gold Nanoparticles, *ACS Appl. Mater. Interfaces*, 2011, **3**(11), 4215–4220.
17 J.-J. Xiong, *et al.*, Colorimetric detection of Cu2+ in aqueous solution and on the test kit by 4-aminoantipyrine derivatives, *Sens. Actuators, B*, 2016, **226**, 30–36.
18 S. Seslija, *et al.*, Cross-linking of highly methoxylated pectin with copper: the specific anion influence, *New J. Chem.*, 2016, **40**(2), 1618–1625.
19 Y. Wang, B. Yan and L. Chen, SERS Tags: Novel Optical Nanoprobes for Bioanalysis, *Chem. Rev.*, 2013, **113**(3), 1391–1428.
20 J. Li, *et al.*, Highly Sensitive SERS Detection of As3+ Ions in Aqueous Media using Glutathione Functionalized Silver Nanoparticles, *ACS Appl. Mater. Interfaces*, 2011, **3**(10), 3936–3941.
21 Y. Ding, *et al.*, Nanomaterial-based optical sensors for mercury ions, *TrAC, Trends Anal. Chem.*, 2016, **82**, 175–190.
22 S. Kamal and T. C.-K. Yang, Silver enriched silver phosphate microcubes as an efficient recyclable SERS substrate for the detection of heavy metal ions, *J. Colloid Interface Sci.*, 2022, **605**, 173–181.
23 C. Wang, *et al.*, Specific and sensitive on-site detection of Cr(VI) by surface-enhanced Raman spectroscopy, *Sens. Actuators, B*, 2021, **346**, 130594.
24 N. Li, J. Ye and Y. Ma, Stimuli-responsive SERS nanoprobes for multiplexing detection, *Sens. Actuators, B*, 2019, **281**, 977–982.
25 T. Yamashita and P. Hayes, Analysis of XPS spectra of Fe2+ and Fe3+ ions in oxide materials, *Appl. Surf. Sci.*, 2008, **254**(8), 2441–2449.
26 I. Singh, X-ray photoelectron spectroscopy studies of Fe3O4 films on Si and MgO substrates grown by pulsed laser deposition, *AIP Conf. Proc.*, 2018, **1942**(1), 080046.
27 A. P. Grosvenor, *et al.*, Investigation of Multiplet Splitting of Fe 2p XPS Spectra and Bonding in Iron Compounds, *Surf. Interface Anal.*, 2004, **36**, 1564–1574.
28 M. Salvadori, *et al.*, Dead biomass of Amazon yeast: A new insight into bioremediation and recovery of silver by intracellular synthesis of nanoparticles, *J. Environ. Sci. Health, Part A: Toxic/Hazard. Subst. Environ. Eng.*, 2017, **52**, 1–9.
29 E. R. Carmona, *et al.*, Green synthesis of silver nanoparticles by using leaf extracts from the endemic Buddleja globosa hope, *Green Chem. Lett. Rev.*, 2017, **10**(4), 250–256.
30 W. Lu, *et al.*, Green synthesis and characterization of superparamagnetic Fe3O4 nanoparticles, *J. Magn. Magn. Mater.*, 2010, **322**(13), 1828–1833.
31 O. u. Rahman, S. C. Mohapatra and S. Ahmad, Fe3O4 inverse spinal super paramagnetic nanoparticles, *Mater. Chem. Phys.*, 2012, **132**(1), 196–202.
32 N. Yetim, *et al.*, Characterization of magnetic Fe3O4@SiO2 nanoparticles with fluorescent properties for potential multipurpose imaging and theranostic applications, *J. Mater. Sci.: Mater. Electron.*, 2020, **31**, 18278–18288.
33 Y. Chi, Synthesis of Fe_3O_4@SiO_2-Ag magnetic nanocomposite based on small-sized and highly dispersed silver nanoparticles for catalytic reduction of 4-nitrophenol, *J. Colloid Interface Sci.*, 2012, **383**(1), 96–102.
34 K. Shameli, *et al.*, Green biosynthesis of silver nanoparticles using Curcuma longa tuber powder, *Int. J. Nanomed.*, 2012, **7**, 5603–5610.
35 A. J. Kora, S. R. Beedu and A. Jayaraman, Size-controlled green synthesis of silver nanoparticles mediated by gum ghatti (Anogeissus latifolia) and its biological activity, *Org. Med. Chem. Lett.*, 2012, **2**(1), 17.
36 T. Theivasanthi and M. Alagar, *Innovation of Superparamagnetism in Lead Nanoparticles*, 2014.
37 L. Tzounis and S. Logothetidis, Fe3O4@SiO2 core–shell particles as platforms for the decoration of Ag

nanoparticles, *Mater. Today: Proc.*, 2017, **4**(7, part 1), 7076–7082.

38 M. Abbas, S. R. Torati and C. Kim, A novel approach for the synthesis of ultrathin silica-coated iron oxide nanocubes decorated with silver nanodots (Fe3O4/SiO2/Ag) and their superior catalytic reduction of 4-nitroaniline, *Nanoscale*, 2015, **7**(28), 12192–12204.

39 S.-S. Chen, *et al.*, A facile ultrasonication assisted method for Fe3O4@SiO2-Ag nanospheres with excellent antibacterial activity, *Dalton Trans.*, 2015, **44**(19), 9140–9148.

40 P. N. Sisco and C. J. Murphy, Surface-Coverage Dependence of Surface-Enhanced Raman Scattering from Gold Nanocubes on Self-Assembled Monolayers of Analyte, *J. Phys. Chem. A*, 2009, **113**(16), 3973–3978.

41 C. E. Talley, *et al.*, Intracellular pH Sensors Based on Surface-Enhanced Raman Scattering, *Anal. Chem.*, 2004, **76**(23), 7064–7068.

42 J. Yan, *et al.*, Highly Sensitive Surface-Enhanced Raman Spectroscopy (SERS) Platforms Based on Silver Nanostructures Fabricated on Polyaniline Membrane Surfaces, *ACS Appl. Mater. Interfaces*, 2012, **4**(5), 2752–2756.

43 F. Bertorelle, *et al.*, Isomeric Effect of Mercaptobenzoic Acids on the Synthesis, Stability, and Optical Properties of Au(25)(MBA)(18) Nanoclusters, *ACS Omega*, 2018, **3**(11), 15635–15642.

44 W. K. H. Ho, *et al.*, Probing Conformation Change and Binding Mode of Metal Ion–Carboxyl Coordination Complex through Resonant Surface-Enhanced Raman Spectroscopy and Density Functional Theory, *J. Phys. Chem. Lett.*, 2019, **10**(16), 4692–4698.

45 Y. Zhang and P. S. Cremer, Interactions between macromolecules and ions: the Hofmeister series, *Curr. Opin. Chem. Biol.*, 2006, **10**(6), 658–663.

46 E. Thormann, On understanding of the Hofmeister effect: how addition of salt alters the stability of temperature responsive polymers in aqueous solutions, *RSC Adv.*, 2012, **2**(22), 8297–8305.

47 Y. Zhou, *et al.*, Colorimetric detection of Cu 2+ using 4-mercaptobenzoic acid modified silver nanoparticles, *Colloids Surf., A*, 2011, **391**(1–3), 179–183.

48 B.-C. Yin, *et al.*, An allosteric dual-DNAzyme unimolecular probe for colorimetric detection of copper(II), *J. Am. Chem. Soc.*, 2009, **131**(41), 14624–14625.

49 Y. Dong, *et al.*, Polyamine-functionalized carbon quantum dots as fluorescent probes for selective and sensitive detection of copper ions, *Anal. Chem.*, 2012, **84**(14), 6220–6224.